Surface Roughness Enhancement of Indirect-SLS Metal Parts by Laser Surface Polishing

J.A. Ramos, J. Murphy, K. Wood, D.L. Bourell, J.J. Beaman

Mechanical Engineering Department
Laboratory for Freeform Fabrication
The University of Texas at Austin, Austin, TX 78712

ABSTRACT

Laser polishing by means of shallow surface melting of indirect-SLS metal parts was achieved using high power CO_2 and Nd:YAG lasers raster scanned at high speed. This was an effective technique for reducing surface roughness. The fast moving laser beam provides just enough heat energy to cause melting of the surface peaks. The molten mass then flows into the surface valleys by surface tension, gravity and laser pressure, thus diminishing the roughness. Surface roughness R_a data were obtained by profilometry measurements of the polished samples. An analytical model was developed based on the assumption that the surface of an SLS part consists of semi-spherical caps. The model was used to predict the R_a values as a function of laser power, scan speed and precursor powder particle size. The modeled results fit the empirical data within a 15% error.

Introduction

For more than a decade the SFF community has acknowledged that the transition from Rapid Prototyping towards Rapid Manufacturing of functional parts requires adequate treatment of surface roughness [1-3]. From a survey carried out by the Laboratory for Freeform Fabrication (LFF) at University of the Texas at Austin, answers from 20 different sources related to RP technology were gathered, indicating that surface finishing is a critical issue when SFF parts need to serve functional purposes. This result was further confirmed in an interview of key people in the RP world published by Time Compression Technologies magazine [4]. On the latter, all interviewed agreed that surface finishing is a major barrier to overcome to achieve functional parts by means of RP.

SLS parts, regardless of the material system used, inherently present a grainy surface finish, which is rough due to powder particle size, layer-wise building sequence and to some degree to the spreading of the powder by the roller mechanisms [5]. The RP survey carried out by the LFF also indicated that among the finishing techniques used today to reduce roughness of SFF parts, surprisingly, hand polishing and abrasive flow grinding were the most commonly used. These are tedious and time consuming, although effective in reducing surface roughness. Less commonly used techniques are electro-polishing, shot-peening, ultrasonic and vibratory finishing [6]. A more sophisticated approach currently used is robotic arm polishing; however, the trajectory of the polishing tool must be determined a priori by 3D profilometry or some other means thus increasing the complexity and cost of this post process [7].

Laser Polishing of Silica Rods

For over 30 years lasers have been excellent tools for material surface modification [8-10]. Depending on the laser processing parameters (i.e., power density and interaction time) several modification regimes can be attained, namely: transformation hardening, melting, glazing, ablation and shock wave generation. Previous work done in the LFF indicated that the surface of silica rods could be polished from 2.0 μm to 0.05 μm (i.e. peak-to-valley distance) by means of a 25 W CO_2 focused c.w. laser [11]. The polishing mechanism is laser melting of a very thin layer of material that flowing under the action of surface tension. A wide laser polishing operational window from 900 to 1300 J/cm^2 existed for this type of material.

Laser Polishing of Indirect-SLS Metal Part

The latter positive results obtained in semiconductor materials encourage pursuing laser polishing of metallic surfaces of SFF parts as made by indirect-SLS technology. High power Nd:YAG and CO_2 lasers (c.w. mode) were successfully used in polishing 420 stainless steel-40 wt.% bronze indirect-SLS parts. Table 1 shows the operation window that provided considerable reduction in roughness R_a values. Figure 1 indicates that the operation window falls inside a melting-welding zone [9].

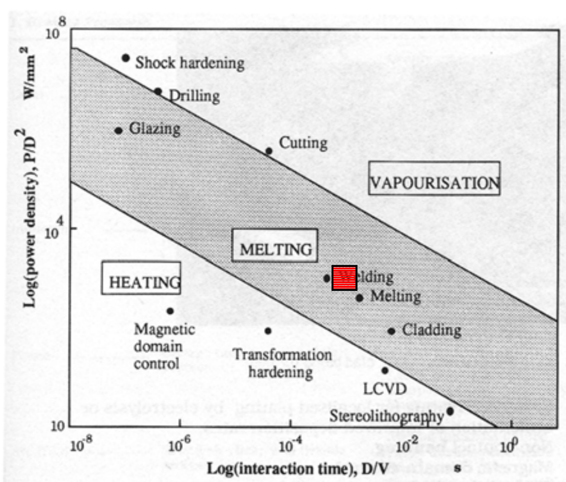

Figure 1. Operational window for several laser processes. Adapted from Steen [9]. The dark box near "Welding" and "Melting" indicates the polishing operational window.

	Max	Min
P [W]	420	220
V_s [m/min]	45	16
P/D^2 [W/mm^2]	$2.7*10^3$	$1.4*10^3$
D/V_t [s]	10^{-3}	$6.5*10^{-4}$

Table 1. Operational window used in laser polishing of indirect-SLS parts. The material system was 420 stainless steel-40 wt.% bronze.

Simplistically, a rough SLS surface can be envisioned as consisting of spherical peaks and valleys. When the laser beam impinges on a rough surface, a peak will have higher probability of reaching the melting temperature before a valley does. A fraction of the molten peak will then flow into the valley by the action of Marangoni forces, gravity and laser pressure [9]. This "partial-melting" mechanism effectively reduces the peak-to-valley height, thus reducing the surface roughness. On the other hand, if the speed of the laser beam is too slow, the peaks may become "over-melted". The surface then becomes completely molten, and it is likely that low frequency - high amplitude surface waves may develop on cooling, thus potentially increasing the roughness.

Experimental Setup

Samples were provided by DTM Corp. and consisted of rectangular slabs made using DTM powder and process development called LaserForm™ ST-100. It consists of a 420 stainless steel mixed with a 2 wt.% polymer binder that is shaped into a green pre-form by means of SLS. The pre-form is then placed inside a N_2 atmosphere furnace to burn off the binder and proceed with a 40 wt.% bronze (5 wt.% Sn) infiltration of the part. This material system is aimed towards tool making for the injection molding industry. The minimum surface roughness achieved is 2.4 μm, but some samples were showing values of up to 9.0 μm depending on the process parameters. Phonak A.G. (Switzerland) has applied this materials system to produce tooling for a hearing aid transmitter housing. However, machining and finishing operations were needed to achieve the specified tolerances [12].

CO_2 and Nd:YAG lasers were used in c.w. mode to laser polish the surface of the samples. The focal spot size of the CO_2 laser was 0.35+/-0.05 mm whereas for the Nd:YAG the real spot size was 0.25+/0.05 mm. High speed galvanometer motor driven rotating mirrors provided scanning speeds of up to 45 m/min raster speed and 2.0 mm/s traverse speed. The processing chamber was evacuated to 200 mTorr and then back filled with a inert gas reducing atmosphere of 4.5%H_2+Ar.

After the samples were treated, the surface roughness of the polished samples was measured using an automated profilometer device. The arithmetic average roughness value (i.e. R_a), was used to quantify this feature. This is the average displacement of the peaks and valleys measured with respect to a mean line.

Empirical Results and Discussion

Figure 2 shows an optical macrograph of multiple CO_2 laser polished tracks. These were made using 220 W and a traverse speed of 2.2 mm/s. The surface roughness R_a value of the as-received sample was 2.1 μm. The achieved surface roughness was brought down to R_a = 1.6 µm (traverse-direction) and R_a = 3.2 µm (scan-direction). The latter value is higher than the as-received because at the overlapped regions a hump is formed. In Figure 3 the transition from the as-received surface to a polished one can be observed. A Nd:YAG laser was used at 220 W and a traverse speed of 1.7 mm/s. The as-received surface roughness R_a value was reduced from 9.0 µm down to a R_a value of 2.40 µm.

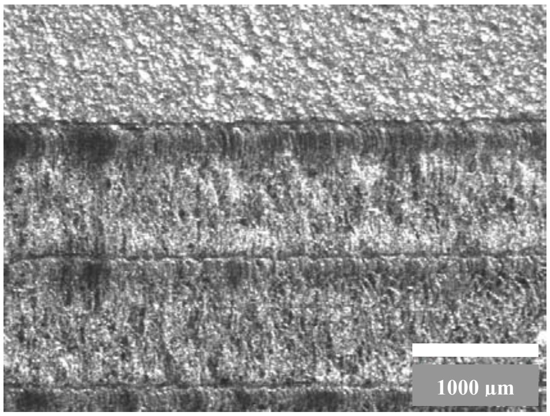

Figure 2. Optical macrograph of multiple CO_2 laser polished tracks on a 420 stainless steel–40 wt.% bronze indirect-SLS slab, 50x.

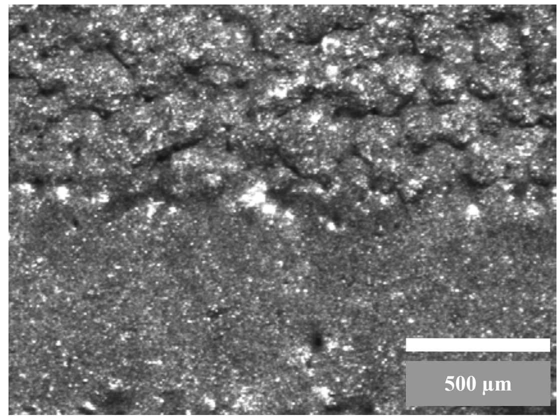

Figure 3. Optical macrograph of Nd:YAG laser polished 420 stainless steel–40 wt.% bronze indirect-SLS slab, 100x.

Figure 4 shows an SEM image of the previous sample, from which it can be clearly seen that the as-received surface is made up of overlapping spherical caps, corresponding to bronze coated 420 stainless steel powder particles and clusters, forming peaks and valleys. Where the laser beam has raster scanned through the sphere caps, these seem to have collapsed down, smoothing the surface. Figure 5 illustrates this better, as it can be seen that at the interface of the as-received and polished zone some sphere caps became semi-melted.

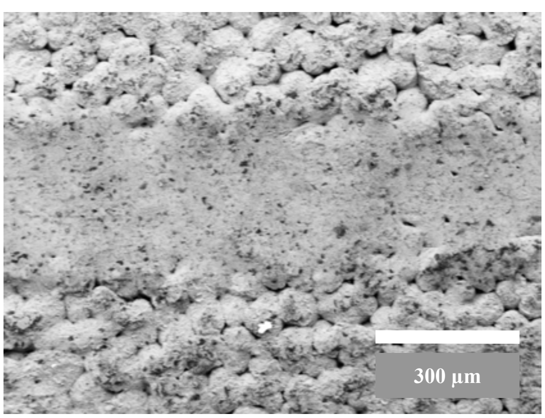

Figure 4 SEM image of Nd:YAG laser polished 420 stainless steel–40 wt.% bronze indirect-SLS slab, 60x.

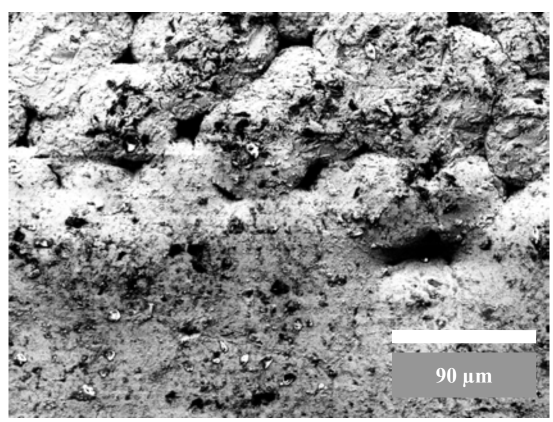

Figure 5 SEM image of interface zone of previous sample, 200x.

Figures 6 (a)-(d) show SEM images of laser polished tracks having widths ranging from 1.8 to 2.9 mm. The difference in resulting track widths is due to the various power and speeds used. The as-received roughness value R_a was 2.38 μm, while the obtained R_a values after polishing were (a) R_a = 0.82 μm, (b) R_a = 1.13 μm, (c) R_a = 2.56 μm and (d) R_a = 4.18 μm. From Figures (a) and (b) in can observed that a higher power provides better polishing results when the traverse speed is fixed. However, Figures (c) and (d) show that for a given laser power, too low a traverse speed produces over-melting with an increase of the R_a value above the as-received level.

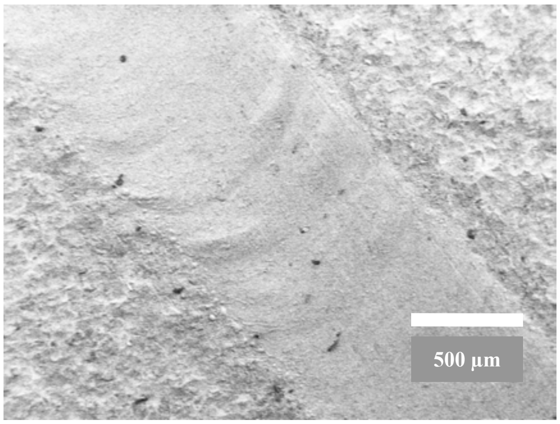

(a) 420 W and 4.5 mm/s, R_a = 0.82 μm

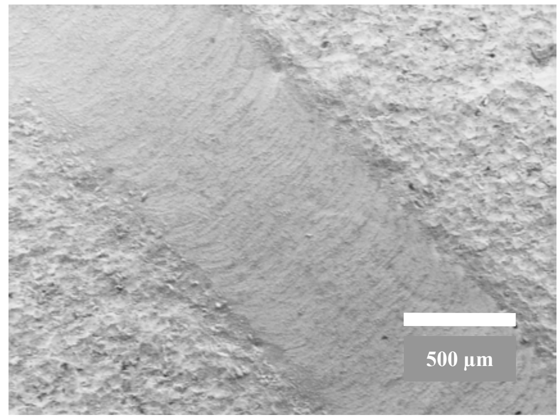

(b) 320 W and 4.5 mm/s, R_a = 1.13 μm

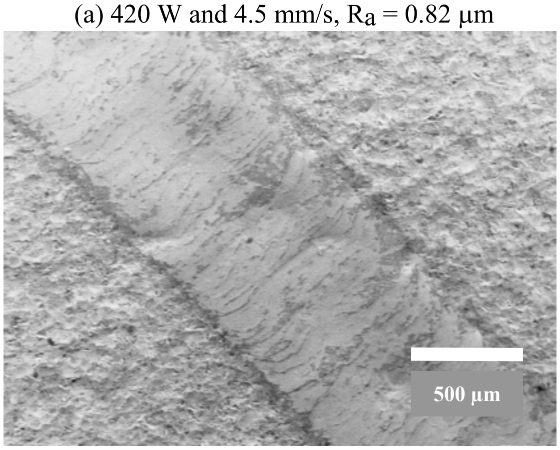

(c) 220 W and 4.5 mm/s, R_a = 2.56 μm

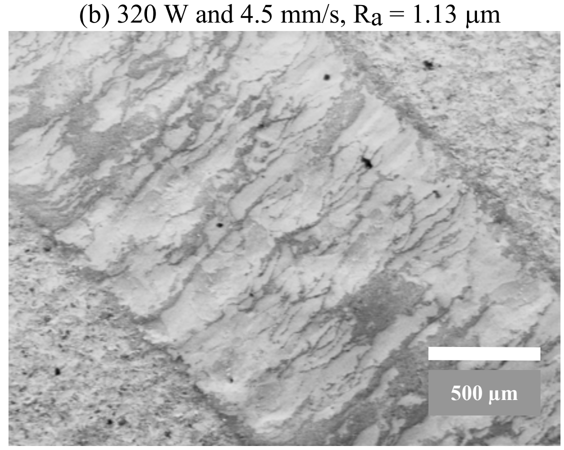

(d) 220 W and 1.8 mm/s, R_a = 4.18 μm

Figure 6. SEM of CO_2 laser polishing of 420 stainless steel–40 wt.% bronze indirect-SLS slab, 50x.

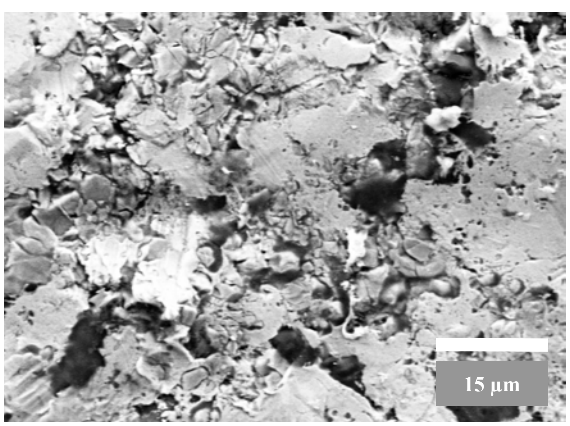

(a) As-received surface, 1500x

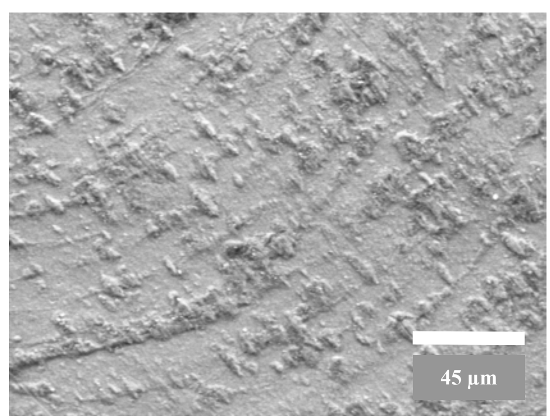

(b) CO_2 laser polished surface, 500x

Figure 7. SEM of as-received and polished 420 stainless steel–40 wt.% bronze indirect-SLS samples.

Figure 7 shows a sequence of SEM images of the surface morphology of laser polished samples. Figure 7a corresponds to the as-received surface having a R_a value of 2.38 μm. Here, powder particles are clearly seen embedded in a bronze matrix. Figure 7b shows a close-up of a polished zone, obtained using 320 W and a traverse speed of 4.5 mm/s. The periodically distributed minuscule humps may have been caused by surface tension and oxidation effects; these contribute to the 1.13 μm roughness R_a measured.

Figure 8 is a plot of the R_a values for Nd:YAG laser polished 420 stainless steel–40% bronze indirect-SLS samples. The power was 220 W at five traversing speeds: 1.46, 1.47, 1.73, 1.74 and 1.76 mm/s. The as-received R_a value of the surface was 9.0 μm, and for the five sets of parameters, a considerable reduction in R_a value was achieved. However, as the speed is increased, the R_a values increase from 3.0-3.3 μm to 3.7-4.1 μm. Higher speed at constant power level implies less melting of the sphere caps and therefore less mass flow into the sphere valleys.

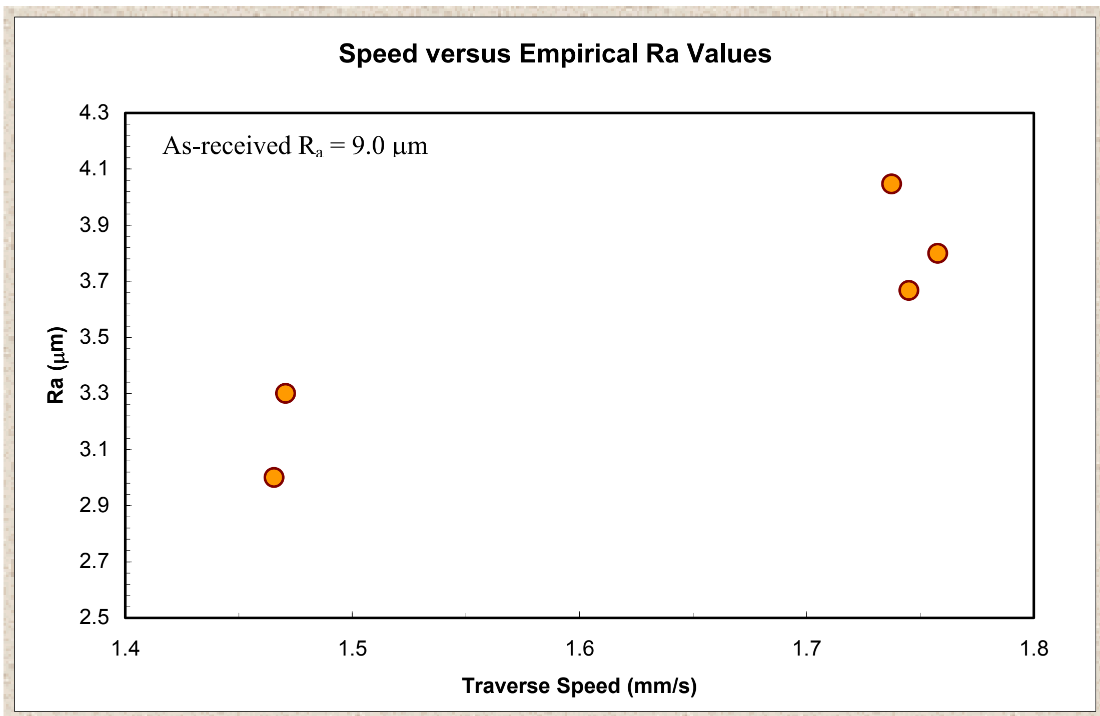

Figure 8. R_a values for Nd:YAG laser polished 420 stainless steel–40 wt.% bronze samples, 220 W.

Figure 9 is a plot of the R_a values for CO_2 laser polishing done at 320 W as a function of traverse speed. In these samples, the as-received R_a value is 2.38 μm, lower than in the previous case. The data show a "U-shape" trend for the R_a values, all below the as-received R_a value, as a function of increasing traversing speed with a minimum R_a of 1.65 μm at 1.19 mm/s. The increase of R_a value with decreasing speed from 1.19 to 0.65 mm/s is attributed to the over-melting mechanism; i.e. the sphere caps are melted completely and surface tension effects and oxidation may possible induce low frequency - high amplitude waviness morphology on the treated surface. In the speed range from

1.19 to 1.89 mm/s the increase in achieve R_a values is due to the partial-melting mechanism as described in Figure 8.

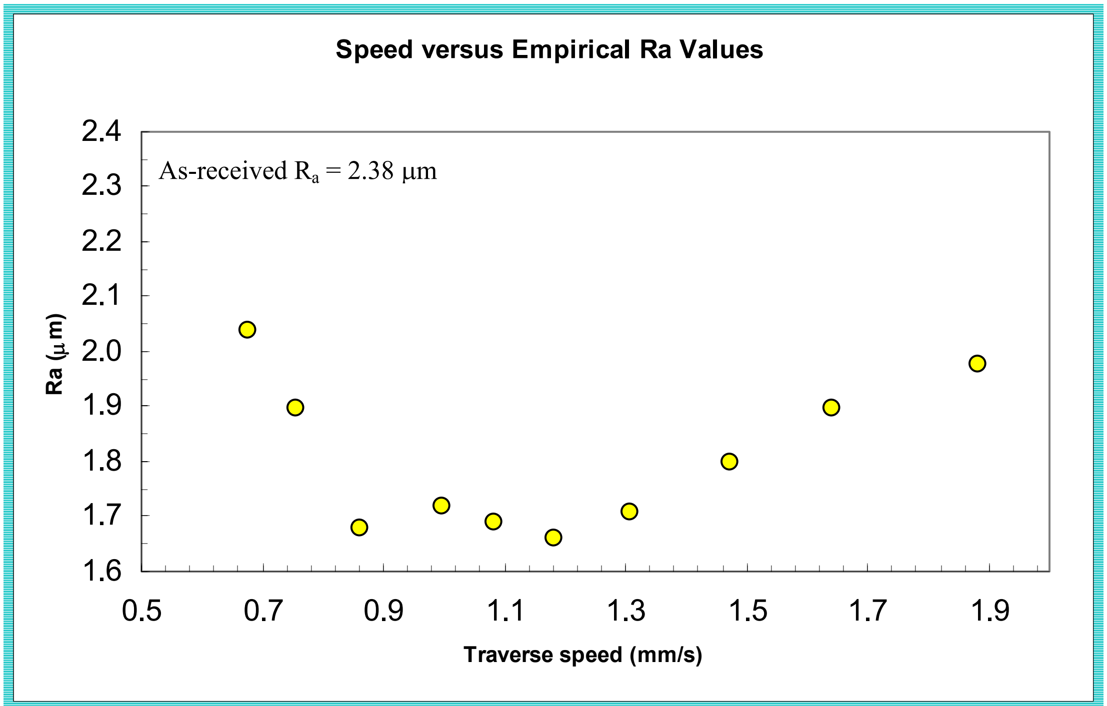

Figure 9. R_a values for CO_2 laser polished 420 stainless steel–40 wt.% bronze samples, 320 W.

Summary of Results

The results obtained indicate that a reduction in R_a roughness has been achieved in 420 stainless steel - bronze infiltrated SLS parts by means of CO2 and Nd:YAG laser polishing. The best results are: (i) R_a reduction from 2.1 µm to 1.6 µm at 220 W and 2.2 mm/s (ii) R_a reduction from 2.38 µm to 1.65 µm at 320 W and 1.19 mm/s and (ii) R_a reduction from 2.38 µm to 0.8 µm at 420 W and 4.5 mm/s. By means of Nd:YAG laser polishing the best result is a R_a reduction from 9.0 µm to 2.40 µm at 220 W and 1.7 mm/s.

Analytical Modeling

Melting Spherical Cap Model

As confirmed by the SEM images, the surface of indirect-SLS metal parts consists of spherical 420 stainless powder particles of different radii that have been coated with bronze during the infiltration process. The surface roughness is then related to the height between the particle peaks and valleys formed in between them. This observation allows us to develop a simple model assuming that the surface is made of tangent semi-spheres as shown in Figure 10a. The impinging coupled laser energy heats up the spherical caps to their melting point with subsequent flow of the melt into the valleys as shown in Figure 10b. The model must be able to determine the newly established surface morphology of the melted caps and filled valleys.

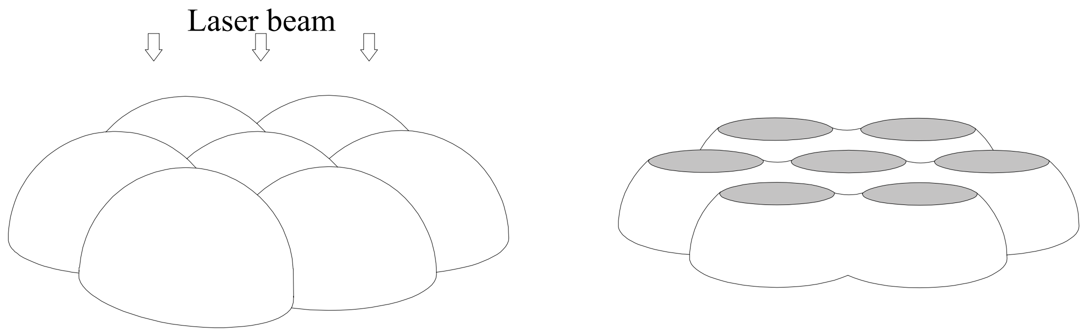

(a) Schematic of spherical cap surface prior to laser impingement on the surface.

(b) Schematic of the surface after the laser has melted the spherical caps.

Figure 10. Assumed sequence of events during laser polishing.

The first step is to write a lumped energy balance, Eq.1, taking into account surface melting and superheating due to a flux of energy (i.e., a stationary laser beam). The energy balance is expressed in terms of the melted volume of one semi-spherical cap, i.e. V_{MELT}. It is then necessary to introduce two parameters f_1 and f_2 (see Figure 11a) to account for the relationship between the thermally affected volume underneath the laser beams, f_1, and the total volume of spherical caps that is melted and superheated by ΔT_l at the surface only, given by f_2.

$$P(1-\Re)\cdot \Delta t_{INTERACTION} = \left[\rho_s Cp_s \Delta T_s \cdot f_1 + (\rho_s L + \rho_l Cp_l \Delta T_l)\cdot f_2\right]\cdot V_{MELT} \quad (1)$$

$$f_1 \propto \left[\frac{\alpha_s \cdot \Delta t_{INTERACTION}}{R^2_{PARTICLE}}\right]^{\frac{3}{2}} \qquad f_2 \propto \frac{D^2_{LASER}}{4\cdot R^2_{PARTICLE}} \quad (2)$$

The time a moving laser beam impinges over a spherical cap, is determined by its own spot diameter and scan speed and is given by Eq.3. This expression is a good approximation for the time a stationary laser beam is heating up the cap surface. Table 2 lists and defines the variables used in equations 1-3.

Variable	Definition	Variable	Definition
P	Laser Power	α_s	Thermal diffusivity of solid phase
$\Re$	Reflectivity	D_{LASER}	Laser spot diameter size
ρ_s	Density of solid phase	$R_{PARTICLE}$	Powder particle radius size
ρ_l	Density of liquid phase	$\Delta t_{INTERACTION}$	Laser interaction time
Cp_s	Heat capacity of solid phase	ΔT_l	Max. temperature above melting
Cp_l	Heat capacity of liquid phase	ΔT_s	Avg. temperature below melting
L	Heat of fusion	$v_{TRAVERSE}$	Traverse speed of laser beam

Table 2. Melting Spherical Cap Model definition of variables.

$$\Delta t_{INTERACTION} = \frac{D_{LASER}}{v_{TRAVERSE}} \tag{3}$$

The volume of a spherical cap expressed as a function of the height, z, measured from its cusp to the basal plane, is given as Eq.4. If this expression is set equal to V_{MELT}, from Eq.1, then the depth of melt, z_m, can be calculated by solving a cubic polynomial on z.

$$V_{CAP}(z) = \frac{1}{3}\pi z^2 \cdot (3R - z) \tag{4}$$

The volume of a sphere segment, $V_{SEGMENT}(z)$ is given as Eq.5. The expression for the volume of a valley to be filled by V_{MELT} is given by Eq.6. The latter was obtained by subtracting the volume of a sphere segment of height z, Eq.5, from the volume of a parallelepiped (i.e. base $4R^2$ and height z), as shown in Figure 11b. To find the filled valley height, z_f, Eq.6 is set equal to Eq.4., the latter evaluated at z_m; this is illustrated in Figure 12a. Again a third order polynomial must to be solved for z_f.

$$V_{SEGMENT}(z) = \frac{1}{6}\pi z \cdot (6R^2 - 2z^2) \tag{5}$$

$$V_{FILLED}(z) = 4R^2 \cdot z\text{-}V_{SEGMENT}(z) \tag{6}$$

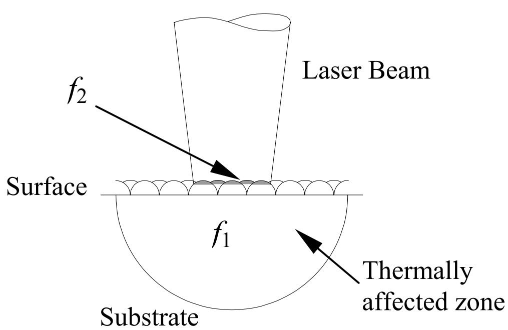

(a) Domain used in lumped energy balance.

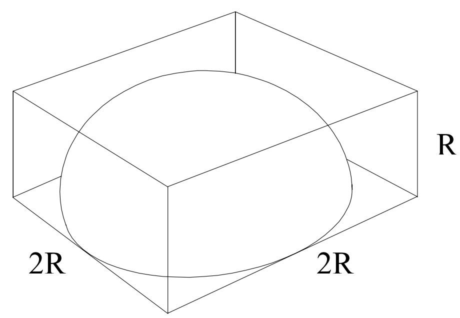

(b) Sphere cap embedded in parallelepiped.

Figure 11. Schematics of the Melting Spherical Cap Model.

Equation 7 gives the expression for the arithmetic average surface roughness as a function of the sphere radii, R_i, corresponding to specific powder particle sizes. This expression computes an arithmetic average between the peak-to-valley distances (i.e. R_i-z_m-z_f) for N different particle sizes (see Figure 12b).

$$R_a \approx \frac{\sum_{i=1}^{N} \frac{(R_i - z_m) - z_f}{2}}{N} \tag{7}$$

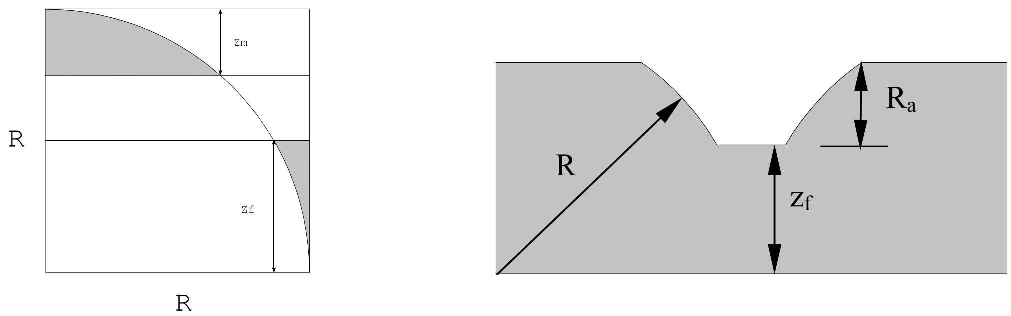

(a) Relationship between melt depth - filled height. (b) Idealized cross section after laser polishing.

Figure 12. Schematic drawings for the determination of the surface roughness R_a value.

From Figure 13 it can be observed that the proposed model fits the empirical data well in the region corresponding to the partial-melt mechanism, i.e. increase in R_a value (below the as-received value) with increasing speed. Particle radii of 10, 15, 20 and 25 µm were considered when computing the R_a values. The model can predict changes in R_a roughness within a 15% error inside an operating window of 1.1 - 1.9 mm/s and 320 W.

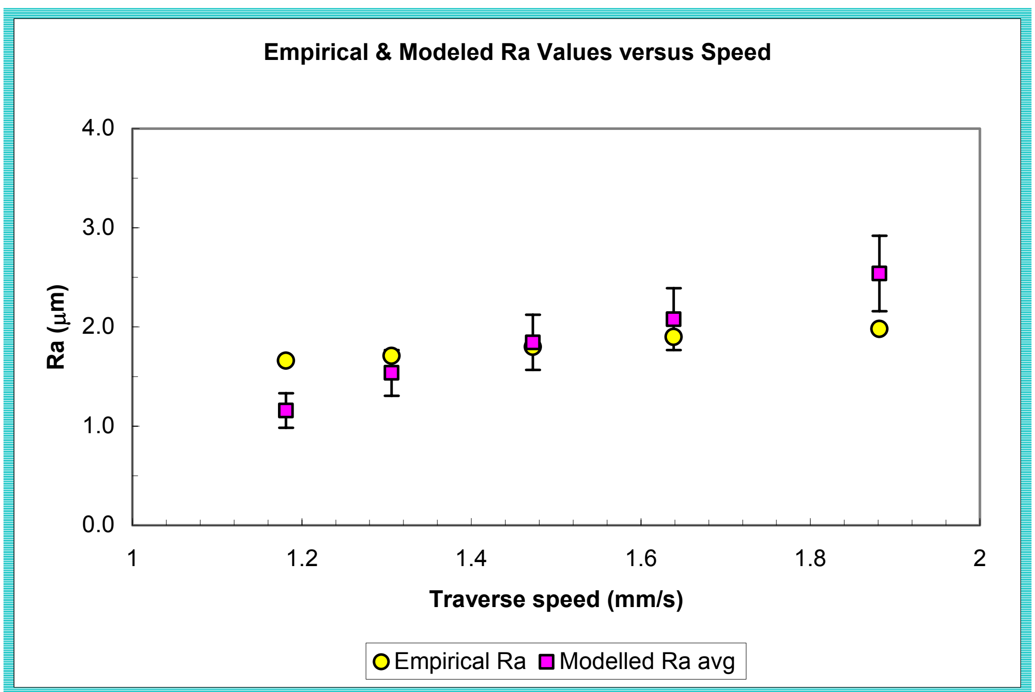

Figure 13. Comparison between measured and modeled R_a values versus traverse speed.

Conclusions

1. Reduction in surface roughness has been achieved by means of a high laser power polishing technique using either CO_2 and Nd:YAG lasers at high scanning speed. Two polishing mechanisms are observed: (a) partial-melting with increase in R_a values with increasing speed, (b) over-melting with decrease in R_a values with increasing speed.

2. As-received surface roughness values affect the reduction in roughness.
3. Surface integrity of the treated part remains to be assessed; however, an increase in the surface microhardness is expected to occur.
4. Laser power and speed control need to be implemented as the parts to be treated have finite dimensions.

References

1. J.J.Beaman, J.W.Barlow, D.L.Bourell, R.H.Crawford (1997): Solid Freeform Fabrication: A New Direction in Manufacturing. Kluwer Academic.
2. M. Burns (1993): Automated Fabrication: Improving Productivity in Manufacturing. Prentice-Hall.
3. J.A. McDonald, C.J. Ryall and D.I. Wimpenny (2001): Rapid Prototyping Casebook, Professional Engineering Publishing.
4. J. Connolly, "Direct Rapid Manufacturing – Is it Possible?", Time Compression Technologies, May, pp. 46-47, 2001.
5. I.Y.Tumer; D.C.Thompson, K.L.Wood and R.H. Crawford, "Characterization of Surface Fault Patterns with Application to a Layered Manufacturing Process", Journal of Manufacturing Systems, Vol. 17, No.1, 1998.
6. J.D. Spencer, R.C. Cobb and P.M. Dickens, "Vibratory Finishing of Stereolithography Parts", Proceedings of the 4th Solid Freeform Fabrication Symposium, Austin, Texas, 1993.
7. D.Shi and I.Gibson: "Surface Finishing of Selective Laser Sintering Parts with Robot", Proceedings of the 9th Solid Freeform Fabrication Symposium, Austin, Texas, pp. 27-35, 1998.
8. J.F. Ready, Ed. (1979): Lasers in Modern Industry. Society of Manufacturing Engineers.
9. W.M. Steen (1994): Laser Material Processing, 2nd edition, Springer Verlag.
10. J.F. Ready, D.F. Farson T. Feeley Eds.(2001): LIA Handbook of Laser Materials Processing, Laser Institute of America, Magnolia Publishing Inc.
11. H.Wang, D.L.Bourell and J.J.Beaman, "Laser Polishing of Silica Rods", Proceedings of the 9th Solid Freeform Fabrication Symposium, pp. 37-45, Austin, Texas, 1998.
12. DTM-Corporation, "Housings for hearing aid transmitter created within two month window". Horizons Q3, pp.5-7, 2001.

Acknowledgments

The Laboratory of Freeform Fabrication gratefully acknowledges the support of the Office of Naval Research for funding the project "Surface Engineering for SFF Processes", Grant Nº: N00014-00-1-0334 and DTM Corporation for providing LaserForm™ ST-100 samples for testing.